Study of Magnetic traps and Radio frequency dressed state potentials

Atul Mantri

A dissertation submitted for the partial fulfilment of BS-MS dual degree in Science

Indian Institute of Science Education and Research Mohali
April 2014

Certificate of Examination

This is to certify that the dissertation titled **Study of Magnetic traps and Radio frequency dressed state potentials** submitted by **Atul Mantri** (Reg. No. MS09033) for the partial fulfilment of BS-MS dual degree programme of the Institute, has been examined by the thesis committee duly appointed by the Institute. The committee finds the work done by the candidate satisfactory and recommends that the report be accepted.

Prof. Arvind | Prof. Jasjeet S. Bagla | Dr. Mandip Singh (Supervisor)

Dated: April 25, 2014

Declaration

The work presented in this dissertation has been carried out by me under the guidance of Dr. Mandip Singh at the Indian Institute of Science Education and Research Mohali.

This work has not been submitted in part or in full for a degree, a diploma, or a fellowship to any other university or institute. Whenever contributions of others are involved, every effort is made to indicate this clearly, with due acknowledgement of collaborative research and discussions. This thesis is a bonafide record of work done by me and all sources listed within have been detailed in the bibliography.

Atul Mantri
(Candidate)

Acknowledgment

While writing this thesis I realized that my time at IISER was one of the most exciting in my life. First I would like to thank Dr. Mandip Singh for providing me an opportunity to work with him. It was a nice experience to have him as supervisor and to learn from him. I would also like to thank Anurag Kulshrestha for his constant discussion throughout the project.

I want to thank my family for their love and support. I thank all of my friends (both inside and outside the institute) for inspiring me in different ways during my stay at IISER. In particular, I want to thank Mariyam Fatima very much for her encouragement. I really enjoyed those endless walks, chats and coffee. I am grateful to Mayank Mishra for introducing me to a lot of different things including field of quantum computing. I thank Abhishek "chotu", Ankush "xxx", Ashima, Harsh, Jithin, Karandeep, Narendra, Neeraj, Nishtha, Nitin, Ravi, Sapna, Shivpal, Vidit etc. for all the discussions. This thesis is dedicated to each and every one of my friends for making this time a memorable one.

Contents

List of Figures

Abstract

The aim of this thesis is to understand and explore radio frequency dressed state potentials for Bose-Einstein condensate. The basic understanding of micro traps use to produce magnetic trapping were first developed. Particularly the U and Z shape wire, which produces 3-dimensional trapping of neutral atoms, were studied in detail. Later on the these trap are combined with rf field of varying polarization. The rf-induced potentials greatly enhances the flexibility and robustness of trapping atoms. For example the double well potential, ring potential and state dependent potential are illustrated. These studies have been used recently in the experiments on matter wave interferometery on an atom chip [1]. In the last section the physics of single particle in periodic potentials is studied. To produce periodic potentials, two different magnetic trap designs are proposed.

Chapter 1

Introduction

This chapter covers background material related to theoretical and experimental concepts behind Bose-Einstein Condensation. The aim of this chapter is to only serve as an overview rather than giving detailed and rigorous proofs. For a more detailed and general reference in this field one can see review papers [2, 3, 4, 5, 6] and book [7].

1.1 Overview of path to BEC

The laser cooling is one of the initial stages to the path for creating BEC, taking atoms from room temperature (few hundred kelvins) to temperature $\sim 50\mu K$. This technique is discussed in the following section. A short description of sub-Doppler cooling, magneto-optical trap and evaporative cooling is also provided in the subsequent sections.

1.1.1 Laser Cooling

This section mostly cover the qualitative description of laser cooling with an overview of Doppler and sub Doppler cooling. In the presence of a laser beam when an atom absorbs a photon, the energy of the photon is converted into the internal state of the atom. The state of the atom is changed from ground state to excited state. This absorption leads to a transfer of momentum to the atom in the direction of photon's initial momentum. Shortly afterwards, atom jumps back to ground state emitting a photon due to spontaneous emission. As we know, due to spontaneous emission, the momentum is released in the random direction. This results in zero net change in the momentum of the atom due to averaging over many absorption and emission cycles. Therefore shining a laser beam on the atom results in change in momentum of the atom in the direction of the laser beam. The magnitude of momentum (of photon) is extremely small, but as on resonance an atom scatters many photons leading to large

forces as a whole. In this process we have assumed that laser is on resonance with the atom. The maximum force on the atom per photon can be given by

$$F = \frac{\Delta p}{\Delta t} = \frac{\hbar k}{2\tau} \tag{1.1}$$

where $\hbar k$ is the momentum transfer to the atom during each absorption-emission cycle which is equal to twice the excited-state lifetime (for the case when atomic transition is saturated such that atom spends half of its time in the excited state).

Doppler Cooling

The above process is used for slowing atoms with light but eventually for cooling one needs to slow down a range of velocity distribution for atoms. One way to do this is to use a force which is both dissipative and velocity-dependent. This technique is also know as *Doppler Cooling* and was first suggested in the paper [8]. Here we explain this technique for one dimensional case i.e. pair of laser beam along only one of the Cartesian axes but it can be easily generalized to three dimensions. Consider an atom moving in the the presence of light such that the light is slightly red-detuned from resonance. As seen in the atom's frame, due to Doppler shift, it sees the light it is moving towards as closer to resonance and the light it moves away is seen as further from resonance. Hence an atom moving in opposite direction to the light is slowed down as scattering of photon is more in this case. The scattering force explained in previous section becomes velocity dependent due to Doppler effect while the spontaneous emission provides the dissipation. Let I be the beam intensity, the the total force is given by

$$F = \hbar k \frac{\Gamma}{2} \left[\frac{I_0}{1 + 2I_0 + 4(\Delta - kv)^2/\Gamma^2} - \frac{I_0}{1 + 2I_0 + 4(\Delta + kv)^2/\Gamma^2} \right] \tag{1.2}$$

where $I_0 = I/I_{sat}$, Γ is the natural line width, and Δ is the detuning from resonance. For the case of red detuning and in the regime $v \sim 0$, the force can be written as

$$F = -\alpha v \tag{1.3}$$

where α is given by

$$\alpha = -4\hbar k^2 s \frac{2\Delta/\Gamma}{[4\Delta^2/\Gamma^2 + 2s + 1]^2} \tag{1.4}$$

This cooling technique is also sometimes called as "optical molasses", first reported in [9]. It is important to note that the force in equation 1.3 is an average and each absorption-emission cycle (spontaneous process) produces heating. This results in

lower limit in Doppler cooling upto which atoms can be cooled, given by

$$T_D = \frac{\hbar\Gamma}{2k_B} \tag{1.5}$$

here, T_D is known as the Doppler temperature.

1.1.2 Sub-Doppler Cooling

There are two important assumptions in the Doppler Cooling which should be taken into account. (due to the observation of sub-Doppler temperatures in experiments) The first is the consideration of atom as two level system rather than multi-level and the second is not taking into account polarisation of the light field. These topics will be qualitatively dealt with in this section.

To start with consider a light of particular polarisation is shined on multi level atom (at rest). There will be population redistribution between the sub-levels that have same energy difference as that of the light field. In other words atom's dipole will orient relative to the polarisation of the field. Introducing a spatially varying polarisation pattern in turn distribute the population level such that the atomic dipole follows the light field. Since there is finite time lag between the orientation of dipole with the polarisation due to time taken for optical pumping between the sub levels. This give rise to sub-Doppler Cooling effects, sometime also know as polarisation gradient cooling.

The limit on the lowest temperature can be achieved is set by the single photon recoil velocity. Therefore, we can define recoil temperature T_R to be:

$$T_R = \frac{(\hbar k)^2}{2mk_B} \tag{1.6}$$

1.1.3 Magnetic-Optical trapping

So far we have discussed the cooling techniques to cool the atoms on the order of their recoil limit (few nK). And the forces in the above techniques were dissipative rather than confining. Now our aim is to produce the force which will trap the atoms while they are being cooled in the experimental apparatus. One of the ways to achieve this is by adding magnetic field (say, one that is produced by anti-Helmholtz coils) to the three interesting pairs of laser beams used for Doppler Cooling. This kind of trap set-up which utilizes a combination of laser and magnetic field for trapping atoms is also know as Magneto-Optical trapping (MOT) [10].

It is useful to consider a simple one dimensional model. Take an atom that has a $F = 0$ground state, and a $F' = 1$ excited state. The magnetic field produced by the anti-Helmholtz coils is quadrupole (in one dimension): zero at the origin, and increases linearly with z. Its direction is such that it always points away from the origin. The atom is illuminated from either side with circularly polarised light in other words red-detuned slightly from resonance. To begin with we will consider just the +z side of the origin. Therefore as we move away from the origin, the Zeeman shift brings the $m_F = 1$ sub-level closer to resonance, and the $m_F = +1$ level further away. Hence an atom will scatter more photons from the σ_- polarised beam coming from the right than it will from the σ_+ beam coming from the left. This results in a force pushing it to the left, towards the origin. Now for the -z side of the origin, the magnetic field points in the opposite direction. The light from the left and right is now σ_- and σ_+ polarised, respectively. Thus the same analogy goes for the -z side resulting in a force that pushes the atom to the right. Therefore, this position dependent restoring force that always pushes atom towards the origin can be used to trap the atoms.

1.1.4 Evaporative Cooling

This method is usually employed as the final cooling stage for preparation of BEC. In this section the principle of evaporative cooling is briefly sketched, for more details we refer to the review paper [11]. This method begins with initially removing atoms exceeding a certain energy. Later the thermalization occurs by elastic collisions of atoms that are left in the trap. As the atoms are evaporated, average energy per atom decreases and hence the gas cools. One way to remove atoms from the trap is by changing trapped states to untrapped states by applying an oscillating magnetic field. All these techniques are routinely used in labs for creating BEC. We will now turn our attention to the theoretical aspects of Bose-Einstein Condensation relevant to the work in this thesis.

1.2 Bose-Einstein Condensation (BEC)

The first experimental observation of BEC was performed more than a decade ago. Since then it opened up and is use to study a variety of research areas. The development after the first BEC goes from studying its fundamental properties to its use in atom interferometry and also to simulate more complex condensed matter system. These are just few of the various fields where BEC is used. This section tries to provide only a short introduction of the theory behind BEC, that too qualitative in most places.

It is easy to think of Bose-Einstein Condensate as a giant matter wave as the phase transition to BEC occurs when there is a macroscopic occupation of a single particle quantum state (usually, ground state). To begin with a more quantitative way to describe phase transition, an atom's spatial extent can be described by its deBroglie wavelength λ_{dB}, for the case of uniform gas of atoms with the number density n,temperature T, is given by

$$\lambda_{dB} = \frac{h}{p} = \frac{h}{\sqrt{2\pi m k_B T}} \tag{1.7}$$

where m is the mass of the atom, h is the Plank's constant, k_B is the Boltzmann constant. Using equation 1.7 that deBroglie wavelength at room temperature is much shorter than the inter particle separation between the atoms, $n^{-1/3}$. But as the temperature is decreased, the wavelength increases and at the point where $n^{-1/3} \approx \lambda_{dB}$, the wavelength of the atoms start to overlap and system undergoes phase transition to a Bose-Einstein Condensation. A single wavefunction of the system is created by the overlap of all atoms. In terms of phase space density of the gas, this transition is attained at $\rho = 1$ where $\rho = n\lambda_{dB}^3$.
Take N non-interacting Bosons trapped in an external 3D harmonic trap where the potential in terms of trap frequency can be written as,

$$V_{ext} = \frac{m}{2}(\omega_x^2 + \omega_y^2 + \omega_z^2) \tag{1.8}$$

The energy levels are given by

$$\epsilon(n_x, n_y, n_z) = \left(n_x + \frac{1}{2}\right)\hbar\omega_x + \left(n_y + \frac{1}{2}\right)\hbar\omega_y + \left(n_z + \frac{1}{2}\right)\hbar\omega_z \tag{1.9}$$

Since in the condensed state, all the atoms occupy ground state of the system. Therefore,

$$\Phi(\vec{r_1}, \vec{r_2}, \ldots, \vec{r_N}) = \prod_i \phi_0(\vec{r_i}) \tag{1.10}$$

where

$$\phi_0(\vec{r}) = \left(\frac{m\omega_{ho}}{\pi\hbar}\right) \exp\left(-\frac{m}{2\hbar}(\omega_x^2 + \omega_y^2 + \omega_z^2)\right) \tag{1.11}$$

where ω_{ho} is the geometric mean of the trap frequencies.

At thermal equilibrium, the average number of particles in a given state can be found using,

$$\langle n(\epsilon)\rangle - \frac{1}{e^(\epsilon - \mu)/k_B T - 1}, \tag{1.12}$$

where $\sum_i \langle n(\epsilon) \rangle = N$ and μ is the chemical potential of the gas. The transition temperature is given by

$$K_B T_c = \hbar \omega_{ho} \left(\frac{N}{\zeta(3)} \right)^{1/3} \tag{1.13}$$

where $\zeta(3) \approx 1.202$ (Reimann Zeta function). At temperature T, the number of the atoms in the condensate, N_0, is given by

$$N_0 = N \left[1 - \left(\frac{T}{T_c} \right)^3 \right]. \tag{1.14}$$

Till now we have assumed gas of bosons to be noninteracting. However experiments are performed with alkali atoms and interaction have to be taken into account. The main effect of these transition if on the density distribution of the cloud and the properties of the condensate rather than the transition temperature or the condensate fraction. The BEC experiments were carried out with alkali gases of low densities ($10^{12} - 10^{15}/cm^3$), therefore only two-body collision are important and that too s-wave. The interaction between the two particles can be written as

$$U(r) = \frac{4\pi\hbar^2 a_s}{m} \delta(r) \tag{1.15}$$

where a_s is the scattering length, m is the mass of the particle. Depending on strength of interaction there are two possible cases: *Weakly interacting bosons* and *Strongly interacting bosons*. Firstly we will study the theory of weakly interacting bosons. Interaction adds a nonlinear term to the Schrödinger equation which can be effectively written as,

$$H = \sum_{i=1}^{N} \left[\frac{\vec{p}^2}{2m} + V(\vec{r}) \right] + \frac{4\pi a_s \hbar^2}{m} \sum_{i<j} \delta(\vec{r_i} - \vec{r_j}), \tag{1.16}$$

with the energy given by

$$E = N \int dr \left[\frac{\hbar^2}{2m} |\Delta\phi(\vec{r})|^2 + V(\vec{r}) |\phi(\vec{r})|^2 + \frac{N-1}{2} \frac{4\pi a_s \hbar^2}{m} |\phi(\vec{r})|^4 \right] \tag{1.17}$$

Defining $\psi(\vec{r}) = \sqrt{N}\phi(\vec{r})$, Eq. 1.17 can be written as

$$E = \int dr \left[\frac{\hbar^2}{2m} |\Delta\psi(\vec{r})|^2 + V(\vec{r}) |\psi(\vec{r})|^2 + \frac{4\pi a_s \hbar^2}{m} |\psi(\vec{r})|^4 \right] \tag{1.18}$$

We need to find out the ground state wavefunction of Eq. 1.18 as we did for non-interacting case (Eq. 1.11). We use a variational method to do this, define a trial

wavefunction for a isotropic harmonic trap,

$$\Psi(r) = \sqrt{N}\left(\frac{m\omega_r}{\pi\hbar}\right)\exp\left(\frac{-m\omega_r r^2}{2\hbar}\right), \tag{1.19}$$

where Ω_r is the parameter to be used in this method, ω_{ho} is the trap frequency. Using Eq. 1.18 and Eq. 1.19, we get

$$E(\omega_r, \omega_{ho}) = N\hbar\left[\frac{3}{4}\left(\omega_r + \frac{\omega_{ho}^2}{\omega_r}\right) + Na_s\sqrt{\frac{m\omega_r^3}{2\pi\hbar}}\right] \tag{1.20}$$

minimizing this with respect to parameter (here ω_{ho}) and rewriting the equation in terms of a_{ho}, where $a_{ho} = \sqrt{\frac{\hbar}{m\omega_{ho}}}$, we get

$$\frac{a_r}{a_{ho}} = \left[1 + \frac{Na_s}{a_r}\sqrt{\frac{2}{\pi}}\right]^{1/4}. \tag{1.21}$$

In Eq. 1.18 if we try to minimize $E - \mu N$ for a fixed μ, then we obtain

$$\left(-\frac{h^2}{2m}\Delta^2 + V(\vec{r}) + \frac{4\pi a_s\hbar^2}{m}|\psi(\vec{r})|^2\right)\psi(\vec{r}) = \mu\psi(\vec{r}) \tag{1.22}$$

This equation is also known as time-independent Gross-Pitaevskii equation.

Also the ratio of the kinetic energy to the interaction energy can be written as

$$\frac{E_{kin}}{E_{int}} \propto \frac{a_{ho}}{N|a_s|}, \tag{1.23}$$

which is very small for large N. Therefore we can neglect the kinetic energy term and this approximation is know as **Thomas-Fermi approximation**. Eq. 1.22 after using this approximation becomes,

$$\mu\psi(\vec{r}) = \left[V(\vec{r}) + \frac{4\pi a_s\hbar^2}{m}|\psi(\vec{r})|^2\right]\psi(\vec{r}) \tag{1.24}$$

And the density of the condensate is by

$$n(r) = |\psi(\vec{r})|^2 == \frac{m}{4\pi a_s\hbar^2}[\mu - V(\vec{r})] \tag{1.25}$$

Chapter 2

Trapping Neutral Atoms on Chips

The possibility to design strongly confining, complex, multi-parameter potentials makes atom chips quite unique. These atom chips are used to study 1D quantum gases [12], atomic beam splitters [13], in quantum information processing [14, 15] and to study several atom-surface interaction where the features of built-in proximity of a surface is required. These atom chips are similar to integrated circuits in various aspects such as miniaturization and integration. The emphasis in this chapter is on the design of magnetic traps from planar distributions and on experimental aspects that are specific to atom chip experiments. Atom chips are used to trap and manipulate atoms using optical traps. But we will only study potentials that are created by magnetic field (static or slowly varying currents) flowing through micro-fabricated wires. In later chapters, we will see different ways to create or modify traps using Radio frequency(RF) potentials, that couples to Zeeman or hyperfine transitions.

2.1 Magnetic traps for neutral atoms

2.1.1 Magnetic Interaction

In the precious chapter we introduced cooling as a step before even creating magnetic traps for atoms. The reason lies in the interaction energy between a neutral atom and a magnetic field. At room temperature even in the fields of the order of many Tesla, the magnetic interaction energy is much weaker than the atom's thermal energy.

To understand the relation between the interaction energy of an atom with a static magnetic field $\boldsymbol{B}$, we consider an atom and choose the basis where the total electronic angular momentum, $\boldsymbol{J}$, and the total electronic angular momentum, $\boldsymbol{I}$, are uncoupled $|J, m_j; I, m_I\rangle$. The hyperfine interaction Hamiltonian for an atom in the ground state is then

$$H = A\boldsymbol{I} \cdot \boldsymbol{J} - \boldsymbol{\mu} \cdot \boldsymbol{B} \tag{2.1}$$

where the first term corresponds to the contribution of the magnetic dipole and the second term is the interaction with the applied magnetic field with magnetic moment, $\boldsymbol{\mu}$ given by

$$\boldsymbol{\mu} = -(\mu_B g_j \boldsymbol{J} + \mu_N g_I \boldsymbol{I}) \tag{2.2}$$

where g_J and g_I are the electronic and nuclear Landé g-factors.//

For alkali metals, the ground state has $L = 0$ and $S = 1/2$, the total electronic angular momentum $J = 1/2$. For ^{87}Rb, which has $I = 3/2$, the total angular momentum F at low magnetic field is a good quantum number and we can use the basis $|F, m_F\rangle$. The Zeeman shift in this region can be approximated to be linear with the magnetic field and therefore the interaction energy of a magnetic dipole with an external magnetic field can written by

$$V(\boldsymbol{r}) = -\boldsymbol{\mu}_m.\boldsymbol{B}(\boldsymbol{r}) = g_F \mu_B m_F B, \tag{2.3}$$

where m_F is the magnetic quantum number, μ_B is the Bohr magneton, g_F is the effective Landé factor of the atomic hyperfine state.

$$g_F = g_J \frac{F(F+1) + J(J+1) - I(I+1)}{2F(F+1)} - \frac{\mu_N}{\mu_B} g_I \frac{F(F+1) - J(J+1) + I(I+1)}{2F(F+1)} \tag{2.4}$$

The second term has a factor $\frac{\mu_N}{\mu_B}$ which is of the order 10^{-3} and can be safely neglected. For ^{87}Rb, the two hyperfine levels which will be used mostly in this thesis are: $|F = 2\rangle$ and $|F = 1\rangle$ having $g_F = 1/2$ and $g_F = -1/2$, respectively.

Depending on the sign of $g_F m_F$, there are two cases possible:

1 $g_F m_F < 0$ (*strong-field seeking state*) : If the direction of the magnetic moment and magnetic field are parallel i.e ($V < 0$), an atom is drawn towards the increasing fields. Minima of the potential are found at the maxima of the field. As the maximum of B corresponds to minimum of potential energy. But according to Maxwell's equation, maximum of the magnetic field is forbidden in free space [16, 17].

2 $g_F m_F > 0$ (*weak-field seeking state*) : If the direction of the magnetic moment and magnetic field are anti parallel i.e ($V > 0$), an atom is drawn towards the minima of the magnetic field. Because a minima of the magnetic field is allowed by the Maxwell's equation, these types of traps are most common for neutral atoms. Although important point to note is that these states are not the state of lowest energy.

2.1.2 Majorana spin-flip transition

As magnetic traps only confine weak-field seeking states, there is a loss of atoms from the traps due to transition from weak-field to strong-field seeking states. These transitions are commonly known as Majorana transitions [18].

One way to ensure whether the trap is stable is to check if atom's magnetic moment adiabatically follows the direction of B (because the atom see a field which is changing in both amplitude and direction). This condition can be written as:

$$\frac{d\theta}{dt} < \frac{\mu_m |\boldsymbol{B}|}{\hbar} = \omega_L \tag{2.5}$$

i.e. in the atom's frame of reference, change of the field's direction must be slow than the Larmor frequency. Thus Atoms confined in a magnetic trap can escape by making spin-flip Majorana transitions due to a breakdown of the adiabatic approximation. This adiabaticity condition is violated in the regions of very small offset field and lead to spin flip transition from trapped states(weak-field seeking) to untrapped states(strong-field seeking).

2.1.3 Static Magnetic Traps

Static magnetic traps can be divided in to two categories, one in which trap minimum is zero magnetic field and another in which there is a finite value of field at the minimum of the trap [19] .

2.1.4 Quadrupole trap

A straight current carrying wire (I_w) cannot form a magnetic field minimum on its own. But if a uniform bias field (B_b) is added in orthogonal direction to the wire, it forms a a 2-dimensional field minimum. This type of trap, commonly known as quadrupole trap, was originally given by Frisch and Segrè in 1933 [20]. The minimum of the field

$$r_0 = \left(\frac{\mu_0}{2\pi}\right) \frac{I_w}{B_b} \tag{2.6}$$

forms along a line parallel to the wire where the bias field cancels the circular magnetic field of the wire. Atoms in the weak-field seeking state can be trapped in this 2-dimensional quadrupole field with the field gradient at r_0 is given by,

$$\left.\frac{dB}{dr}\right|_{r_0} = \frac{B_b}{r_0}. \tag{2.7}$$

Parameters for Quadrupole trap:

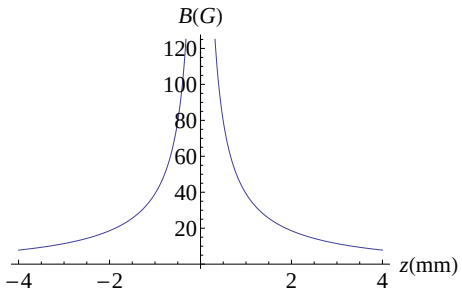

(a) Magnetic Field due to single wire

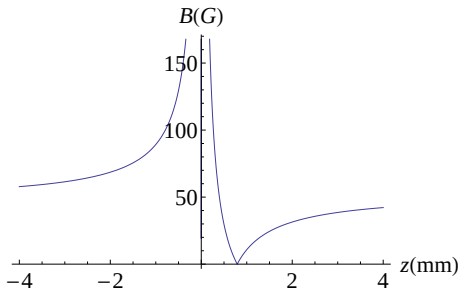

(b) Bias field + field due to single wire

Figure 2.1: Quadrupole trap from single wire and uniform bias field.

$I_w = 20A$, $B_b = 50G$, $B_{\min} = 0$, $B'_{\min} = 63.2\text{G/mm}$ at $r_0 = 0.79\text{mm}$

The miniaturization of the magnetic field sources, wires in this case, results in much larger magnetic fields, field gradients and field curvatures. This is in contrast to conventional magnetic traps created from large field coils which require hundreds of amps to achieve similar parameter but the trap volume of the these coil based traps is large as compared to wire traps.

Due to zero minimum field at the trap center, trapped atom loss due to Majorana transition. This can be minimized by reducing the temperature of the atoms. Another way in which this problem is circumvented is by using second class of static magnetic traps.

2.1.5 Ioffe-Pritchard trap

The other types of traps which can have finite value of field at trap center are known as Ioffe-Pritchard (IP) traps. The idea for these type of trap was first suggested and demonstrated by Pritchard [21, 22] and also is related to Ioffe configuration discussed several years ago for plasma confinement [23]. Although the field was generated from combination of macroscopic wire which in turn creates a harmonic trap at the trap center. Nowadays any trap which generates field configuration of this type is termed as IP trap .

We can see that adding a magnetic field (offset), B_{ip}, along the wire direction lifts the minimum value of magnetic field from zero to some finite value at the trap center. There is no confinement along the wire. Note that the finite value turns out to be exactly equal to B_{ip} (offset field). This also changes the potential form of the trap

near the minimum from linear to harmonic. The curvature is given by

$$\left.\frac{d^2B}{dr^2}\right|_{r_0} = \frac{B_b^2}{r_0^2 B_{ip}} \tag{2.8}$$

and the trap frequency can be written as

$$\omega = \frac{1}{2\pi}\sqrt{\frac{\mu_B g_F m_F}{M}\left(\frac{d^2B}{dr^2}\right)} \tag{2.9}$$

where M is the mass of the atom.

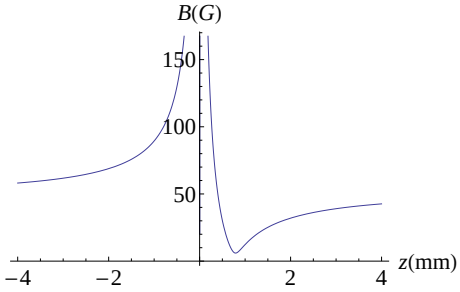

Figure 2.2: IP trap created using single wire, uniform bias and offset field.

Parameters for IP trap:

$I_w = 20A$, $B_b = 50G$, $B_{ip} = 6G$, $B_{\min} = 6G$, $B''_{\min} = 651.04\text{G/mm}^2$, $\omega = 131.68\text{Hz}$ at $r_0 = 0.79\text{mm}$

It is interesting to note that the Majorana losses present in the quadrupole traps can be avoided by using these kind of trap configuration where there is finite value of field at the minimum. Due to Landau-Zener transition from a trapped to untrapped state, probability of atom loss for IP traps is given by:

$$\Gamma_M = 4\pi\omega \exp\left(-\frac{\omega_{\text{Larmor}}}{\omega_{\text{ho}}}\right) \tag{2.10}$$

For parameters given above, the flip rate is practically negligible.

2.1.6 "U" and "Z" - shape wire - magnetic micro traps

The traps described in the previous section constitute only 2-dimensional trapping whereas for practical purpose we will also need to confine the atoms in the third dimension. One of the ways to extend a 2-dimensional to a 3-dimensional trap using the above tools is to make wires in the shape of U and Z [24, 25]. In this section we will see how these two wire configuration generate magnetic confinement along the

free dimension in the aforementioned wire.

The U trap is formed by bending the straight wire from the ends in the shape of "U" such that the opposite current flows in the end wires. Whereas if the wires are bent in the shape of "Z" and current flows in the same direction, it forms a Z trap. Current flows equal in all the three ends of the U or Z wires. These bent shaped parts give rise to 3-dim minimum at the trap center with zero and finite value of field in case of U and Z trap, respectively. The potential form at the trap center are analogous to 2-dim quadrupole and IP trap discussed above. In the following section, it is shown how the magnetic field(its derivative and curvature) varies near the trap center (for U and Z wire). The variation of trap frequency with width, height, current and bias field in the wire are plotted along different axes.

Plots for U Wire

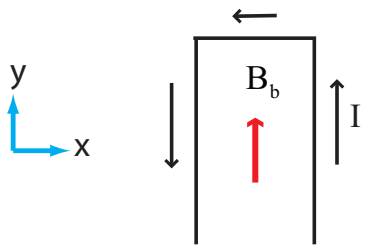

Figure 2.3: U Wire

length of center wire	5 mm
length of side wire	20 mm
width	.5 mm
height	1 mm
current	10 A
Bias field	20 G

Axes	Field Gradient (B/mm)
x	0.09
y	4.52
z	15.84
+45 deg	22.3
−45 deg	12.31

Trap Center for this wire configuration : $\{0, 0.26\text{mm}, 0.91\text{mm}\}$

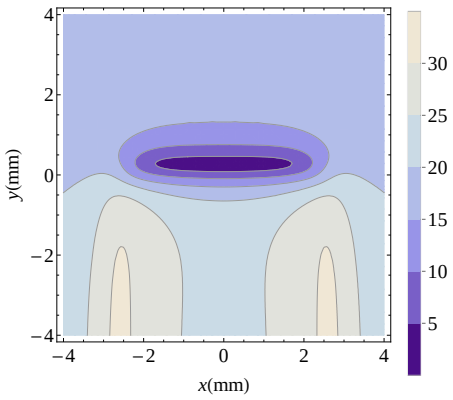

(a) Contour Plot for U trap

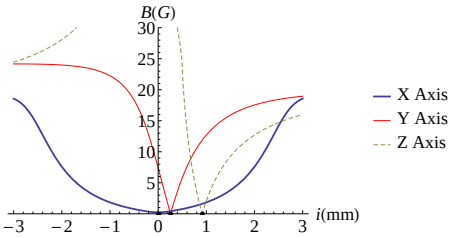

(b) Magnetic field along X,Y,Z Axes

Figure 2.4: Field Plot showing trap center for U wire

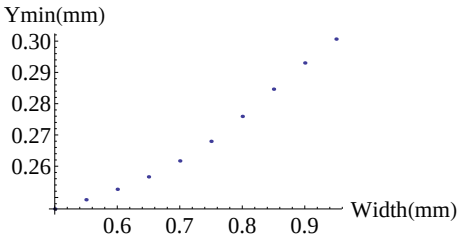

(a) Umin Vs width

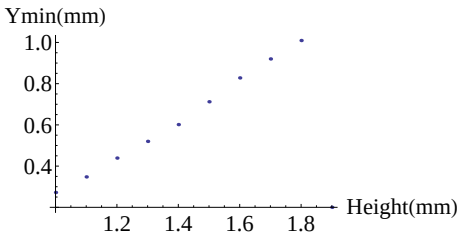

(b) Umin Vs height

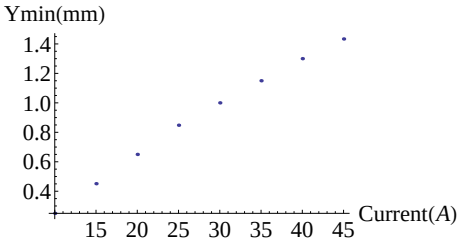

(c) Umin Vs Current

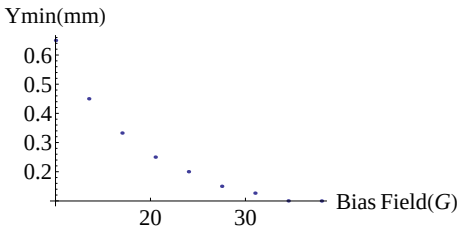

(d) Umin Vs Bias field

Figure 2.5: Variation of Ymin with U wire parameters for Z trap

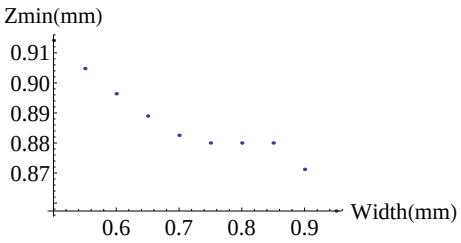

(a) Zmin Vs width

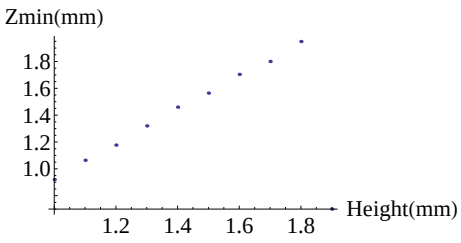

(b) Zmin Vs height

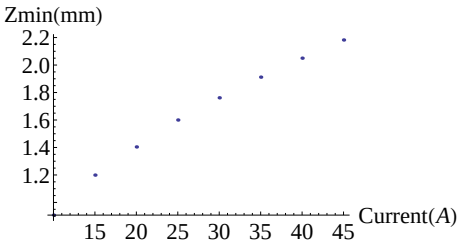

(c) Zmin Vs Current

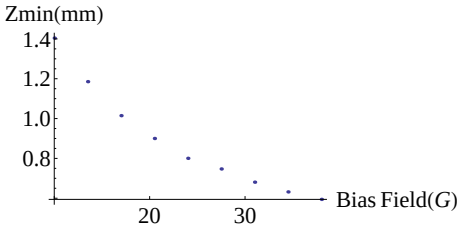

(d) Zmin Vs Bias field

Figure 2.6: Variation of Zmin with parameters for Z trap

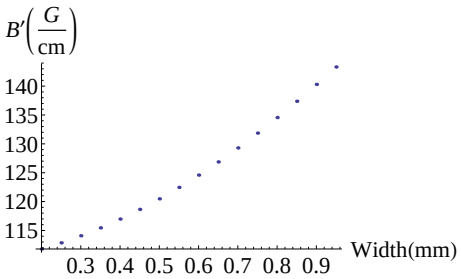

(a) Field gradient Vs Width

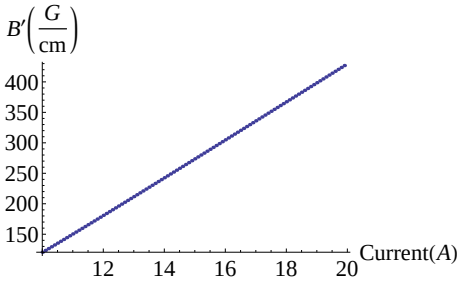

(b) Field gradient Vs Current

Figure 2.7: Variation of field gradient along 45 deg with trap parameter

Plots for Z Wire

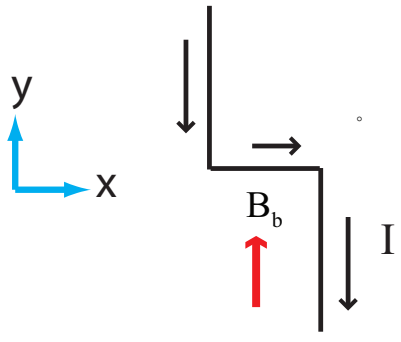

Figure 2.8: Z Wire

length of center wire	5 mm
length of side wire	20 mm
width	.5 mm
height	1 mm
current	10 A
Bias field	20 G

Axes	Trap. freq (Hz)
x	25.23
y	48.22
z	97.34
axial	198.09
radial	326.26

Trap Center for this wire configuration : $\{0, 0, 1\text{mm}\}$

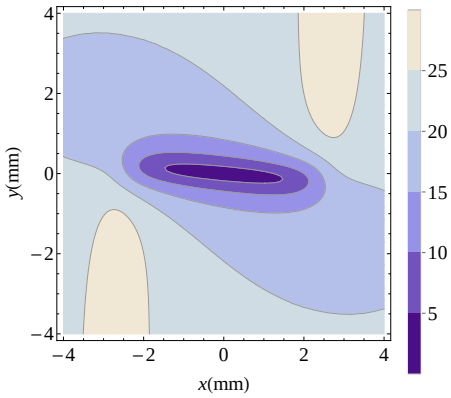

(a) Contour Plot for Z trap

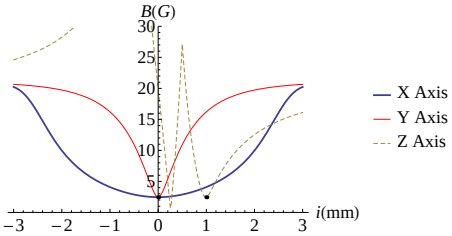

(b) Magnetic field along X,Y,Z Axes

Figure 2.9: Field Plot showing trap center for Z wire

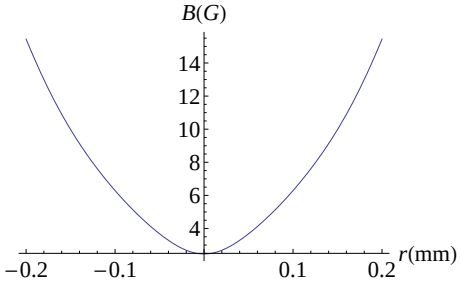

(a) Magnetic field along radial direction

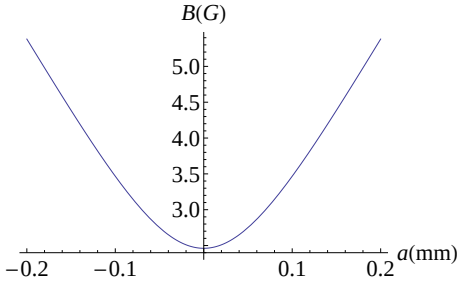

(b) Magnetic field along axial direction

Figure 2.10: Plot for Z trap

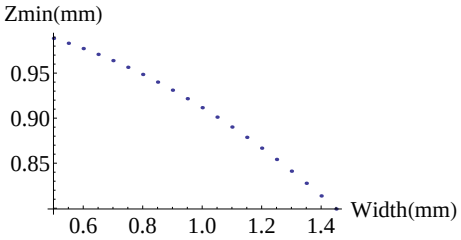

(a) Zmin Vs width

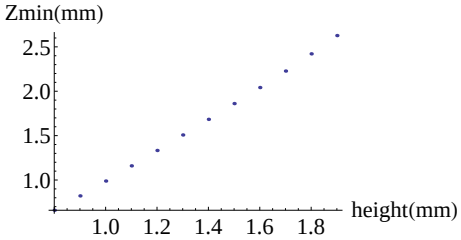

(b) Zmin Vs height

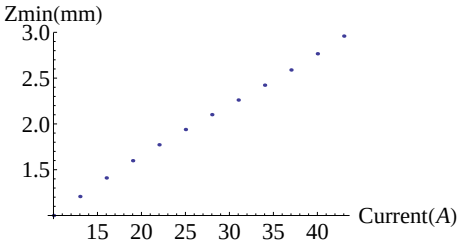

(c) Zmin Vs Current

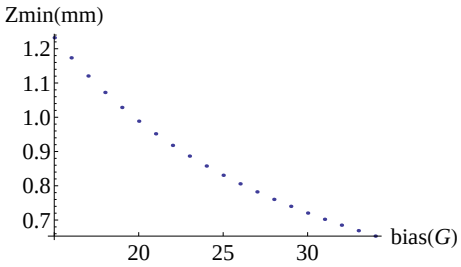

(d) Zmin Vs Bias field

Figure 2.11: Variation of Zmin with parameters for Z wire

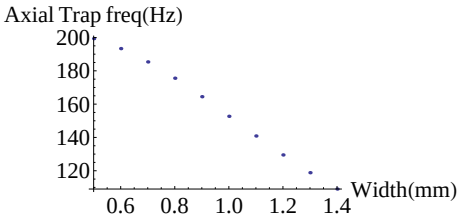

(a) Axial trap freq. Vs width

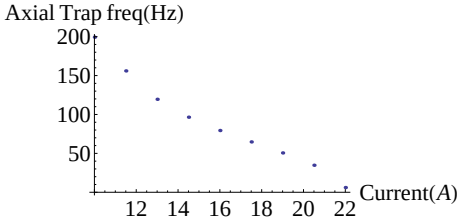

(b) Axial trap freq. Vs Current

Figure 2.12: Variation of trap freq. along axial direction with parameters for Z wire

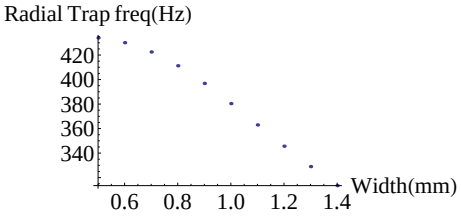

(a) Radial trap freq Vs width

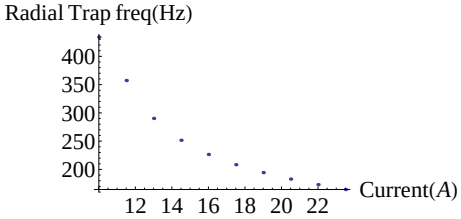

(b) Radial trap freq Vs Current

Figure 2.13: Variation of trap freq. along radial direction with parameters for Z wire

+

Chapter 3

Radio-frequency dressed state potentials

In the previous chapter we have discussed 2 and 3-dimensional magnetic trapping of neutral atoms with static magnetic fields. We have also seen that weak-field seeking states (energetically higher than strong-field seeking states) are the ones which are trapped.

In this section the effect of RF dressing on traps is studied. This procedure is analogous to coupling of different electronic states of a trapped atom using a laser beam in optical traps. Therefore to study our problem we will use *dressed state* picture originally developed by S. Haroche and C. Cohen-Tanoudji in the 1960s. This approach can be found in textbook [26]. It gives a full quantum mechanical treatment of an atom in a field where both field and atom are quantized. We will not use the quantum treatment but will describe the potential by treating radiation field classically. These potentials are referred to here as rf-dressed potentials.

By coupling hyperfine levels of the electronic ground state by a magnetic radio-frequency field or microwave field, dressed state potentials can be studied(in neutron optics [27]). For example, the RF coupling have been proposed to modify potentials in [28] and a detuned microwave has been used for Cs atoms [29]. Similarly, adiabatic potentials from RF has been proposed for neutrons [30] and experimentally performed for the case of Rb atoms [31].These RF dressed state potentials have also been used recently for coherent splitting of a BEC and matter-wave interference experiments [1].

3.1 Interaction of a two level atom with an oscillating field

In this chapter and hereafter in the thesis we will consider atom to be two level, for simplicity, although the same procedure can be extended for atoms with three level and higher. The two levels are labelled as $|0\rangle$ and $|1\rangle$ with energies E_1 and E_2 ($> E_1$), respectively. This atom interacts with the oscillating magnetic field such that total Hamiltonian of the system can be written as $H = H_0 + H'$ where H' and H_0 are the Hamiltonian due to interaction and atom respectively. We will first introduce a semi-classical approach where the atomic levels are quantised while the field is classical. Later on we will see the full quantum picture by quantising the field.

3.1.1 A semi-classical approach

The field is taken to be of the form of $A\cos(\omega t)$ where A is the amplitude and ω is the frequency. A two level atom state for this atom is taken to be

$$|\psi\rangle = c_1 e^{-i\omega_1 t}|1\rangle + c_2 e^{-i\omega_2 t}|2\rangle \tag{3.1}$$

where $|1\rangle$ and $|2\rangle$ are lower and higher energy state with energy $\hbar\omega_1$ and $\hbar\omega_2$ respectively. Inserting this state and total Hamiltonian ($H = H_0 + H'$) in the time-dependent Schrödinger equation

$$i\hbar\frac{d|\psi\rangle}{dt} = H|\psi\rangle \tag{3.2}$$

we get

$$i\hbar\dot{c}_1 e^{-i\omega_1 t}|1\rangle + i\hbar\dot{c}_2 e^{-i\omega_2 t}|2\rangle = H'(c_1 e^{-i\omega_1 t}|1\rangle + c_2 e^{-i\omega_2 t}|2\rangle) \tag{3.3}$$

On simplifying the above equation, we get

$$i\hbar\dot{c}_1 = \langle 1|H'|1\rangle c_1 + \langle 1|H'|2\rangle c_2 e^{-i\omega_0 t} \tag{3.4}$$

$$i\hbar\dot{c}_2 = \langle 2|H'|1\rangle c_1 e^{i\omega_0 t} + \langle 2|H'|2\rangle c_2 \tag{3.5}$$

where $\omega_0 = \omega_2 - \omega_1$.

Therefore, we define $M_{ij} = \langle i|H'|j\rangle$ and can be written as

$$M_{ij} = \hbar\Omega_{ij}\cos(\omega t) \tag{3.6}$$

where Ω_{ij} is the *Rabi* frequency which incorporates the amplitude of the matrix ele-

ment. The equations can now be rewritten in terms of Rabi frequency as

$$i\dot{c}_1 = \frac{\Omega_{12}}{2}c_2(e^{-i(\omega_0-\omega)t} + e^{-i(\omega_0+\omega)t}) + \Omega_{11}c_1\cos(\omega t + \phi_1) \tag{3.7}$$

$$i\dot{c}_2 = \frac{\Omega_{21}}{2}c_1(e^{i(\omega_0-\omega)t} + e^{i(\omega_0+\omega)t}) + \Omega_{22}c_2\cos(\omega t + \phi_2) \tag{3.8}$$

We will now introduce the so called Rotating Wave Approximation (RWA). There are two terms in the above equations containing frequencies of $\omega_0 \pm \omega$. If we assume that the $\omega_0 \approx \omega$ i.e. detuning is small then terms containing $\omega_0 + \omega$ can be neglected with respect to $\omega_0 - \omega$ as the former term is rotating faster than the latter. Applying the RWA to above set of equations and writing them in the form of matrix, we get

$$i\frac{d}{dt}\begin{pmatrix} c_1 \\ c_2 \end{pmatrix} = \frac{1}{2}\begin{pmatrix} 0 & \Omega e^{-i(\omega_0-\omega)t} \\ \Omega^* e^{i(\omega_0-\omega)t} & 0 \end{pmatrix}\begin{pmatrix} c_1 \\ c_2 \end{pmatrix} \tag{3.9}$$

The energies of the state can be calculated solving the above equations as eigenvalue problem

$$U = \pm\frac{\hbar}{2}\sqrt{\delta^2 + \Omega^2} \tag{3.10}$$

where $\delta = \omega - \omega_0$ is the detuning and the eigenstates corresponding to these energies can be written as

$$|\psi_+\rangle = \frac{1}{\sqrt{2\Omega^2 + 2\delta^2 + 2\delta\sqrt{\delta^2+\Omega^2}}}\begin{pmatrix} \delta + \sqrt{\delta^2+\Omega^2} \\ \Omega \end{pmatrix} \tag{3.11}$$

$$|\psi_-\rangle = \frac{1}{\sqrt{2\Omega^2 + 2\delta^2 + 2\delta\sqrt{\delta^2+\Omega^2}}}\begin{pmatrix} -\Omega \\ \delta + \sqrt{\delta^2+\Omega^2} \end{pmatrix} \tag{3.12}$$

These results are analogous to a system where two levels are spaced by an energy δ and is subject to a perturbation of strength Ω. Since the total Hamiltonian is time independent. If we treat the radiation as a single mode, quantum field, rather than the classical field as considered in previous section, energy levels may be introduced to represent the total (atom + field) system and the atom may be regarded as moving in these time-independent potentials. The following case is best described using the figure 3.1, we have consider the field to be quantized. The first two columns of the the figure shows the energy levels of the two parts of the system that are are uncoupled. These states are called bare states and are shown for both positive detuning. Here the energy levels of the two-level atom are denoted by $|1\rangle$ and $|2\rangle$, and radiation field by $|n\rangle$, which form a ladder of states whose energies depend on the number of photons in the field. Whereas in the last part of the figure, the energy levels are shown taking interaction into account. These states are called as dressed states, denoted by $|i, n\rangle$ where the first index is for atoms and second for field. We will consider detuning to

be small so that these states are very close to each other, separated by δ as shown in figure. The interaction is shown using Ω, in the case of $\Omega = 0$ these states are bare states while for finite interaction there is a increase in separation between the states from δ to $\sqrt{\delta^2 + \Omega^2}$.

We can define a rotation matrix such that it maps the bare states onto the dressed states. For example, if we define $|1, n\rangle$ and $|2, n-1\rangle$ to be the initial two level basis states, the dressed states can be written as

$$\begin{pmatrix} |\psi_+\rangle \\ |\psi_-\rangle \end{pmatrix} = \begin{pmatrix} \cos\theta/2 & \sin\theta/2 \\ -\sin\theta/2 & \cos\theta/2 \end{pmatrix} \begin{pmatrix} |1, n\rangle \\ |2, n-1\rangle \end{pmatrix} \tag{3.13}$$

where $\theta = \arctan(\Omega/\delta)$.

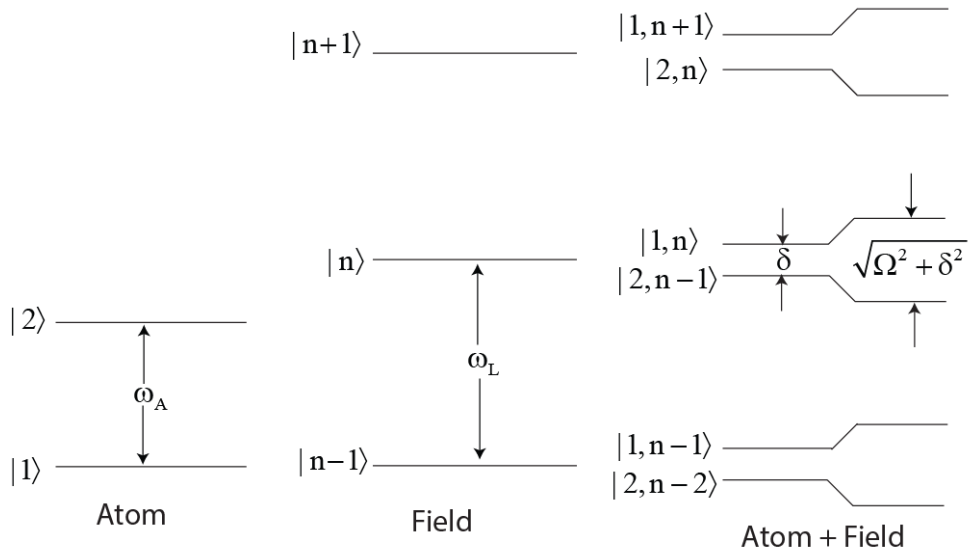

Figure 3.1: Dressed State for the case of positive detuning

3.1.2 Avoided Crossing

It is interesting to note that if the detuning is positive instead of the negative then two energies of the two state would have swapped. When the detuning is zero i.e. $\delta = 0$ then the two levels are degenerate for zero interaction while for $\Omega \neq 0$ the two states will not be degenerate for any detuning. Therefore there is an avoided crossing as shown in figure 3.2.

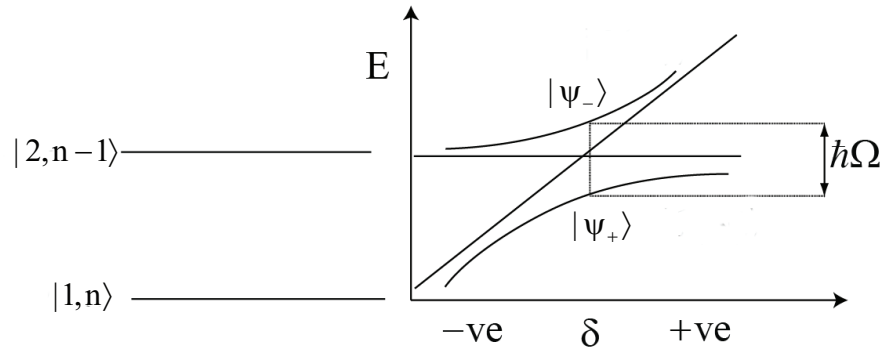

Figure 3.2: Avoided Crossing

3.2 Simulations of RF potential for Z trap

In this section we will cover the implementation of radio frequency (rf) potentials, we have discussed so far, on an atom chip. We will see how the spatial degree of freedom in both the detuning and Rabi frequency of the rf potential is exploited using the precise control and the strong field gradients of traps. We will study the the rf potential for a set-up which consist of three current carrying wires in the shape of Z, an external bias field, together which creates Ioffe-Pritchard type field configuration and two linear rf fields of same frequency as shown in 3.3. We will show the analytic expressions for the resulting rf-potentials for this trap as derived in [32, 33, 34]. We will explicitly show how the shape of the potential depends on the phase shift between the two rf fields. Also we will see the double well and ring like potential arising from linear and circular polarized case, respectively. Later we will discuss the more general case of elliptic polarization of the total rf field and will show how a state dependent double well arises in this case. Particularly in this case, the rf-potentials also depend on the g-factor of the trapped atoms and hence can be use to realize a state dependent potential.

3.2.1 Analytic calculations

For simplicity, we will restrict the calculation of rf potential realized with Z wire by considering field which approximate the real wire field around the trap center (static). In the case of realistic scenarios it is shown that wire magnetic fields will only change the quantitative picture of the rf-potentials whereas qualitatively it remains same.

The magnetic field for a Z trap near its trap center can be written as,

$$B_S(r) = G\sqrt{x^2+y^2}[\cos\phi \boldsymbol{e}_x - \sin\phi \boldsymbol{e}_y] + B_o \boldsymbol{e}_z \tag{3.14}$$

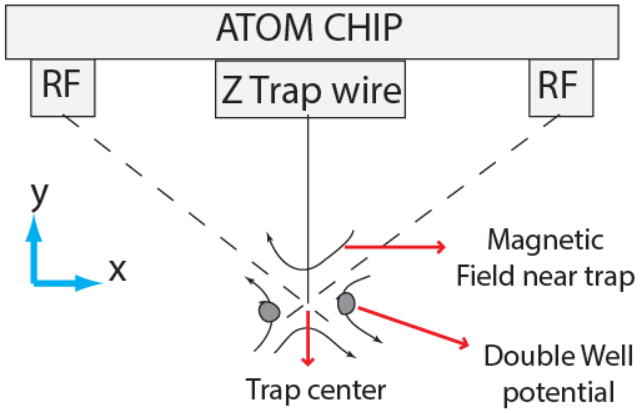

Figure 3.3: Atom chip setup for RF-potentials

where $\phi = \arctan\frac{y}{x}$. The above expression can be seen as a quadrupole field with gradient G in the plane perpendicular the main wire (center) of the Z-wire and a constant offset field (as seen in previous chapter) with amplitude B_o.

The rf field can be written as the superposition of two perpendicular linear field, in general

$$B_{rf} = [B_A \boldsymbol{e}_x + B_B \exp(i\delta)\boldsymbol{e}_y] \exp(\omega_{rf} t) \tag{3.15}$$

where δ is the phase shift between the two components of the rf field. Using the toolbox we developed in earlier section we can solve 3.14 and 3.15 to calculate rf-potentials. To give a brief overview of steps, firstly we diagonalize the the static field term (i.e. field for Z-trap) by applying an unitary transformation U_s which will transform the total spin operator of the atom such that it remains non-zero only in one direction (say z-component). The final potential can be written as,

$$V_{rf} = m_F g_F \mu_B \sqrt{\Delta(r)^2 + \Omega(r)^2}, \tag{3.16}$$

where the $\Delta(r)$ is the detuning and $\Omega(r)$ is the Rabi frequency given by

$$\Delta(r) = |B_s(r)| - \frac{\hbar\omega_{rf}}{|g_F \mu_B|} \tag{3.17}$$

$$\Omega^2(r) = \frac{B_A^2 + B_B^2}{8B_S^2}\Big[2B_o[B_o + |B_S|\sin(2\alpha)\sin\gamma] + G^2(x^2+y^2)[1-\cos(2\alpha)\cos(2\phi)+\sin(2\alpha)\sin(2\phi)\cos\gamma]\Big] \tag{3.18}$$

here, $\tan(\alpha) = \frac{B_B}{B_A}$ and $\gamma = -\frac{g_F}{|g_F|}\delta$ is the effective phase shift and can be seen to be dependent on the sign on the g-factor (which becomes important in elliptic polarization case).

Now we will consider three cases where the rf field is linearly, circularly or elliptically polarized.

3.3 Linear Polarization

In this case we take the phase shift between the two components i.e. $\delta = 0, \pi$. Therefore the Rabi frequency can be written as,

$$\Omega^2 = \frac{|B_{rf}|^2}{8|B_S|^2} \times \left[2B_o^2 + G^2\rho^2 f(\phi)\right] \tag{3.19}$$

where we have defined, $\rho = \sqrt{x^2+y^2}$ and $f(\phi) = 1-\cos(2\alpha)\cos(2\phi)\pm\sin(2\alpha)\sin(2\phi)$. The sign of the third term in the $f(\phi)$ comes from the fact that δ can be 0 or π. This function has two minima in the range of $[0, 2\pi]$. This minima's are located at α, $\alpha+\pi$ ($-\alpha$, $-\alpha+\pi$) for $\delta = 0$ (π). We have plotted rf potential in this case for different

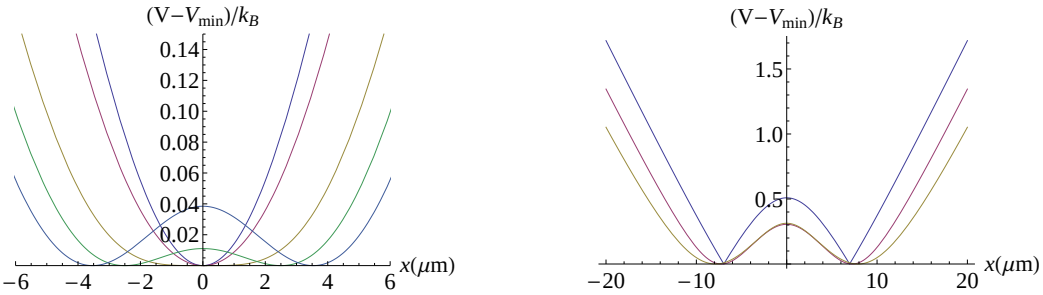

(a) Positive detuning (b) Negative detuning

Figure 3.4: RF-potentials created for the case by linear polarization

rf field amplitudes in case of both positive and negative detuning. In the figure 3.4a, for the case of positive detuning if $|B_{RF}|$ is less than a critical field, B_C, then there is a minima at $x = 0$. And when the $|B_{RF}|$ increased such that it becomes greater than B_C, the minima moves away from the origin and a double well is formed. On the other hand if the rf field frequency is increased such that detuning becomes negative in that case potential takes the form as shown in the right hand side of figure 3.4b.

The rf potential always has minima and takes the form of double well irrespective of strength of rf field. Also, the orientation of the double well is determined by the direction of the rf field. This is illustrated in the contour plots below where the dark blue color shows the position of the minima.

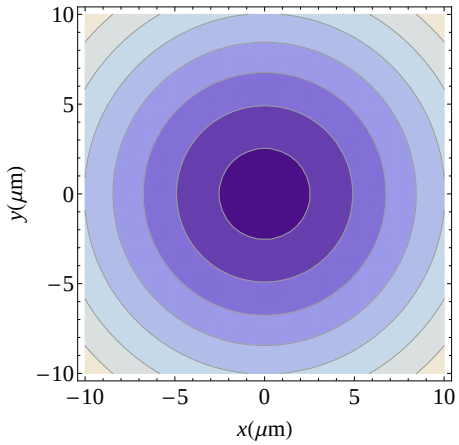

(a) $B_{RF} = 0$ and $\delta = 0$

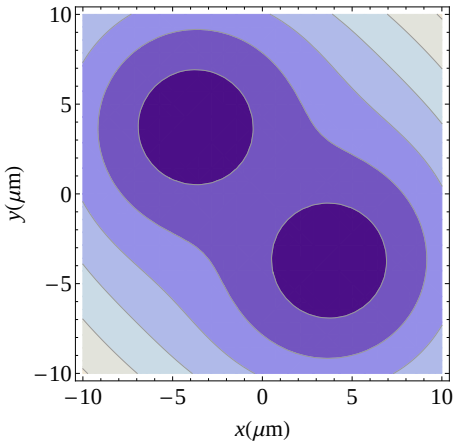

(b) $B_{RF} = 3$ and $\delta = 0$

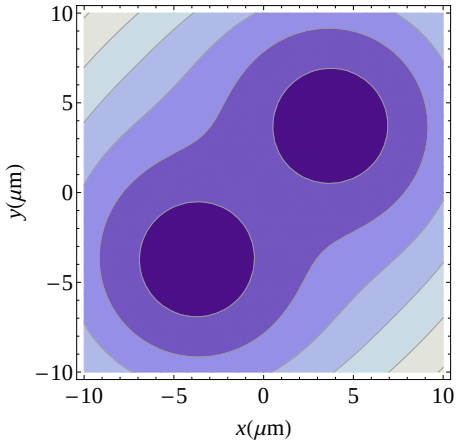

(c) $B_{RF} = 3$ and $\delta = \pi$

Figure 3.5: Contour Plot for linear rf polarization at different B_{RF}

Therefore, depending on the polarization either the potential remains at the same position with a slight change in shape or it can shift the minimum position and convert into a double well potential. This has been particularly used in the paper [1] where the authors have used the double well potentials to demonstrate the splitting of BEC into two clouds having access both to tunnelling and isolated regimes. And then they show the deterministic phase evolution throughout the splitting process by analysing the interference patterns of the condensates.

3.4 Circular Polarization

In this case, the phase shift between the components is taken to be $\pi/2, 3\pi/2$ but with the condition that the amplitudes of both the components are equal. Therefore, $\delta = \pi/2, 3\pi/2$ and $B_A = B_B$ which in turn implies $\alpha = \pi/4$. Putting values of these angles into 3.18,

$$\begin{aligned}\Omega^2(r) &= \frac{|B_{rf}^2}{8|B_S|^2}\left[2B_o[B_o \pm |B_s| + G^2(x^2+y^2)\right] \\ &= \frac{|B_{rf}^2}{8|B_S|^2}(|B_S| \pm B_I)^2\end{aligned} \tag{3.20}$$

The sign in equation 3.20 depends on the effective phase shift. For $\gamma = \pi/2, -3\pi/2$ $(-\pi/2, 3\pi/2)$ the expression takes $+(-)$ sign. Therefore in addition to the value of the phase shift between different components of the rf field, the sign of the g-factor also becomes important in determining the resulting rf potential.

Here again there are two possible scenarios: positive detuning and negative detuning. The rf potential for the first case is shown in the figure 3.6. In the case when $B_{rf} = 0$ then independent of γ, the plot obtained is shown in figure 3.6a. It is interesting to note that when B_{rf} is increased then for the case when $\sin(\gamma) = -1$ we get the same plot whereas when $\sin(\gamma) = 1$ then minimum moves away from the origin (once B_{rf} is more than a critical field strength) making it a ring trap as shown in fig. 3.6b.

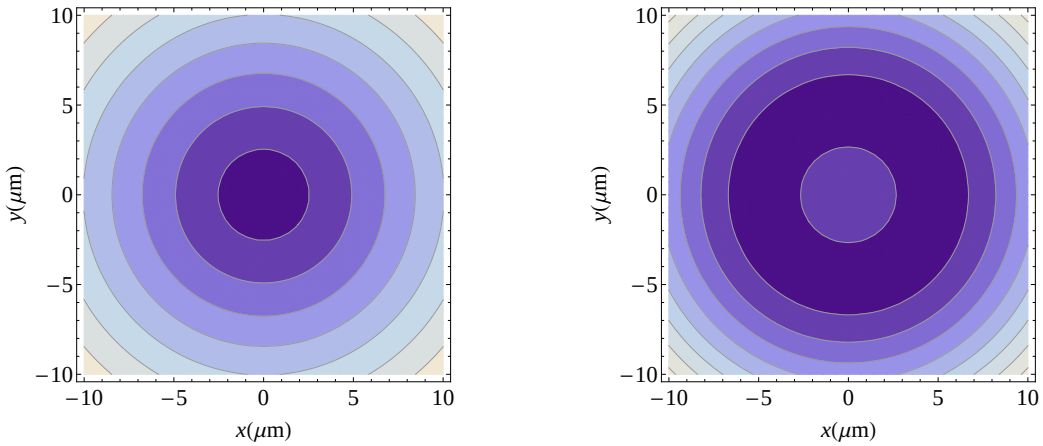

(a) $B_{RF} = 0$ and $\delta = 0$ (b) $B_{RF} = 2$ and $\delta = 0$

Figure 3.6: Contour Plot for circular polarization at different B_{RF}

In the second case when detuning is negative there is always a minima at non-zero x(similar to the case of linear polarization) and is independent of γ. In this case the

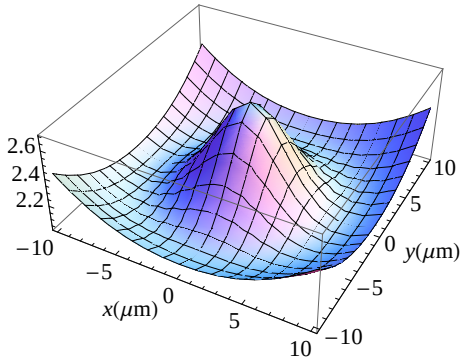

Figure 3.7: Ring potential at $B_{RF} = 3$ and $\delta = 0$

rf potential is ring shaped for any value of rf field strength.

3.5 Elliptic Polarization

In this section, same phase shift between the different component of the rf field is taken as in the case of circularly polarized rf field but with the condition that $B_A \neq B_B$. Hence in this case the total rf field is elliptically polarized. In the previous section we saw that rf potential is dependent on the sign of g-factor apart from phase shift. Similarly for arbitrary polarization also, potential changes with the sign if g-factor. This feature is used for state dependent manipulation of atoms. To exploit this effect, we use two states (hyperfine) of ^{87}Rb i.e. $|F = 2, m_F = 1\rangle$ and $|F = 1, m_F = -1\rangle$ such that they have same μ ($= m_F g_F \mu_B$) value but with different g-factor. If $B_{rf} = 0$ i.e. only static field is present then these two states will see the same potential. As the value of rf field (elliptically polarized) is increased the resulting potential will be different for both the states. In the figure 3.9 an elliptically polarized rf field creates a double well potential for one state whereas as the atom in the second state sees a single minimum.

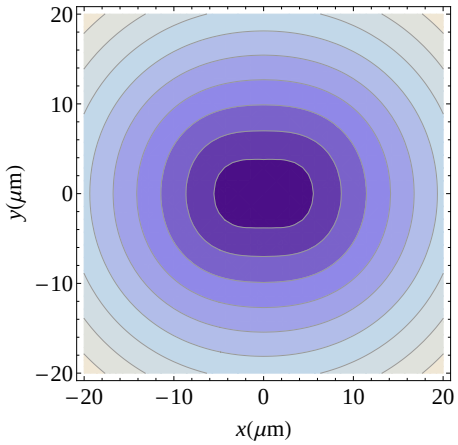

(a) $B_{RF} = 0$ and $\delta = 0$

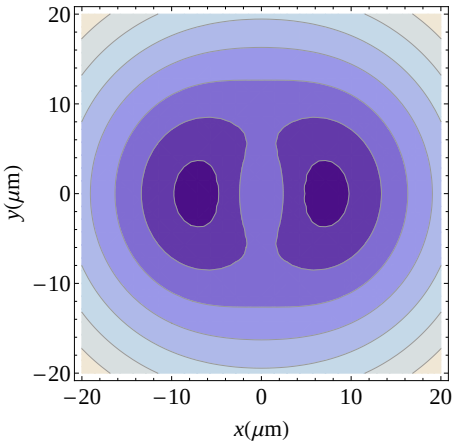

(b) $B_{RF} = 3$ and $\delta = 0$

Figure 3.8: Contour Plot for Elliptic rf polarization at different B_{RF}

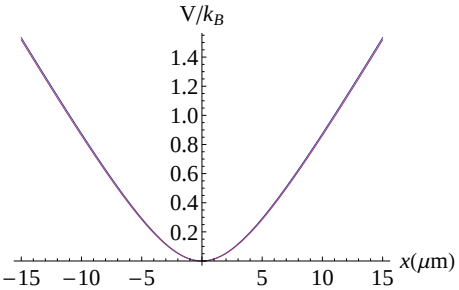

(a) $B_{RF} = 0$ and $\delta = 0$

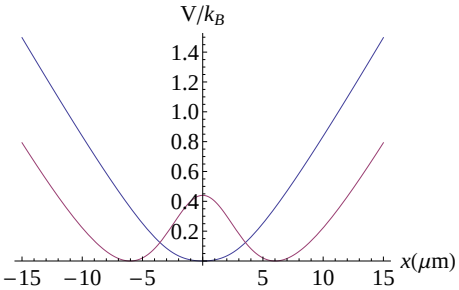

(b) $B_{RF} = 2.2$ and $\delta = 0$

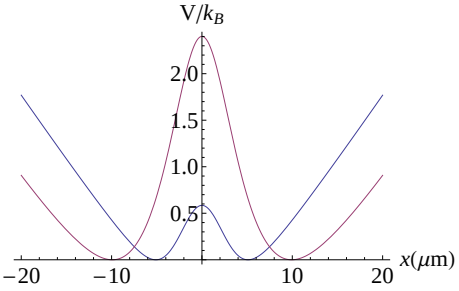

(c) $B_{RF} = 4$ and $\delta = 0$

Figure 3.9: State dependent potential created by elliptic polarization

Chapter 4

Design of circular lattice of magnetic traps

4.1 Single particle in a periodic lattice

In this section we are going to study the dynamics of an atom in an array of periodic lattice. This will be useful later once we will propose a design of circular magnetic trap lattice and use the machinery developed in this section for further analysis.

To begin with we subject the particle to a periodic lattice/potential and discuss the basics that describe the dynamics of this particle. For the sake of simplicity we will consider the problem to be one-dimensional, one can generalize to higher dimension using similar arguments.

The Hamiltonian of a particle can be written as

$$H = \frac{p^2}{2m} + V_{\text{lattice}} \tag{4.1}$$

where $V_{\text{lattice}}(x)$ is periodic lattice with period a. According to Bloch's theorem [35] the eigenstates, $|\phi_q^n(x)\rangle$, can be chosen such that it has two parts: plane wave and a periodic function with period same as of the potential. Using this theorem and Schrödinger equation we obtain:

$$H|\phi_q^n(x)\rangle = E_q^n|\phi_q^n(x)\rangle \tag{4.2}$$

where $\phi_q^n(x) = \exp(iqx)u_q^n(x)$ and $u_q^n(x)$ is periodic function with period a. Putting

this form of eigenstate in the 4.2 yields

$$\left[\frac{(p+\hbar q)^2}{2m} + V_{latt}\right] u_q^n(x) = E_q^n u_q^n(x)\rangle \tag{4.3}$$

For example, if we consider the potential of the form :

$$V(x) = V_0 \sin^2(kx) \tag{4.4}$$

On putting this equation in Schrödinger equation, we obtain a differential equation

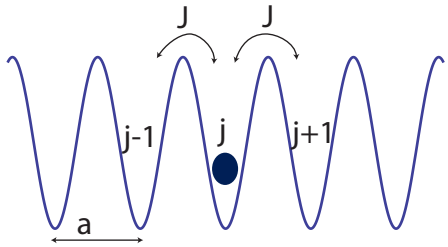

Figure 4.1: Atom in a periodic potential

of the form

$$\frac{d^2}{dy^2}\phi_q(y) + \left[\left(\frac{E_q}{E_R} - \frac{V_0}{2E_R}\right) + 2\left(\frac{V_0}{4E_R}\right)\cos(2y)\right]\phi_q(y) = 0 \tag{4.5}$$

where $E_R = \hbar^2 k^2/2m$ and $y = kx$. Figure 4.2 shows the band structure for the periodic lattice of form given by (4.4) for different depth.

Similarly, the probability density of the ground state wavefunction is plotted for different V_0. The dashed part in the figures show the potential and thick part shows the probability of particle in these potential. It can be clearly seen from the plots that as the depth of potential is increased the amplitude of the wavefunction decreases in between the adjacent sites.

Note that if there is no potential, $V_x = 0$, then the solutions are plane waves (as shown in above figures).

We are interested to analysis particle in periodic potential created by magnetic traps. First considered the Hamiltonian for a boson in a potential [36] as

$$H = \sum_j \epsilon_j \hat{n}_j - J \sum_{<ij>} b_j^\dagger b_i \tag{4.6}$$

where $b_i(b_i^\dagger)$ are boson annihilation (creation) operator at site i(i), $\hat{n}_i = b_i b_i^\dagger$ is the number operator. Here the first term contributes to single particle energy, the second to the tunneling between nearest neighbours. To study inter site tunneling for periodic

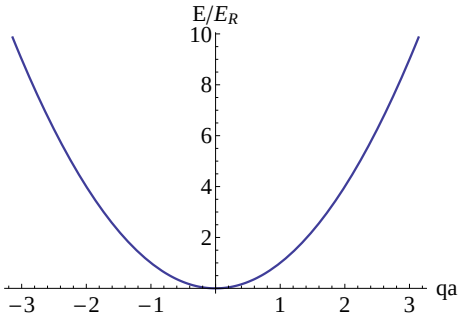

(a) $V_0 = 0$

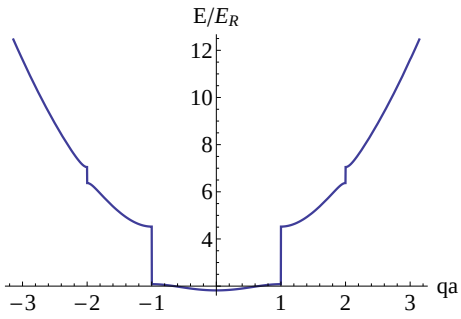

(b) $V_0 = 5E_R$

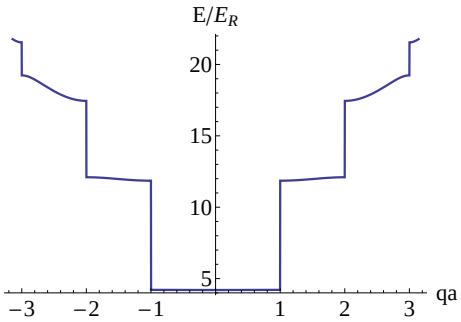

(c) $V_0 = 20E_R$

Figure 4.2: Band Structure of atom in a periodic lattice for different V_0

potential, we will ignore terms carrying ϵ_j. Therefore

$$H = -J \sum_j (|x_j\rangle\langle x_{j+1}| + |x_{j+1}\rangle\langle x_j|), \tag{4.7}$$

and

$$H|\phi_q\rangle = E_q|\phi_q\rangle \tag{4.8}$$

where $|\phi_q\rangle = \sum_j \exp(iqx_j)|x_j\rangle$. Form 4.7 and 4.8, the lowest energy band of the dispersion relation can be shown to have the form:

$$E_q = -2J\cos(qa) \tag{4.9}$$

4.2 Designing unique circular array of magnetic traps

Our aim is to calculate dispersion relation for different potential created from magnetic field. We also want to study the effect of distance between adjacent sites and depth of lattice on the tunneling coefficient, For this purpose, we propose two different designs to create circular array of magnetic traps.

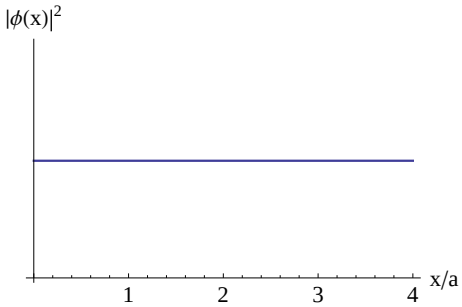

(a) $V_0 = 0$

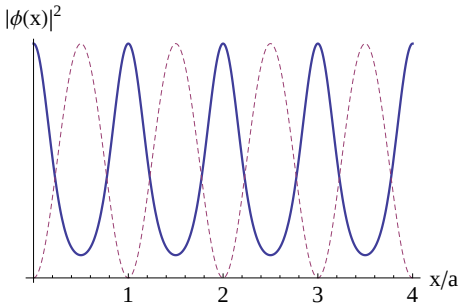

(b) $V_0 = 5E_R$

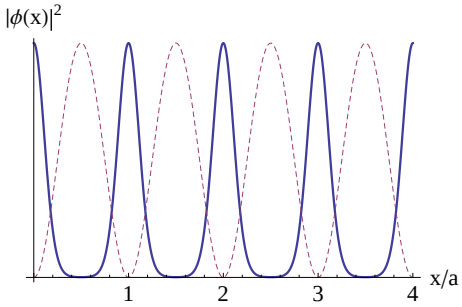

(c) $V_0 = 20E_R$

Figure 4.3: Probability density of particle in periodic potential for different V_0

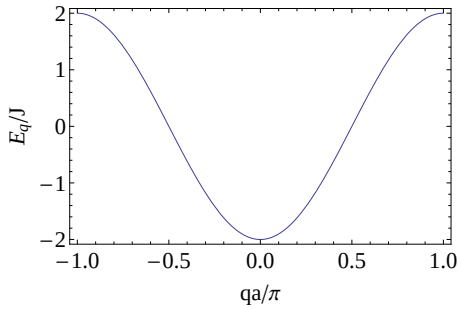

Figure 4.4: Dispersion relation

4.2.1 Magnetic trap I

Here we consider 11 side wires joined in shape of Z in the x-y plane. Center wire along z-axis is in the middle of this setup as shown in the fig. 4.5. Current in the side wire is 10A while in the center wire it is 25A. The trap center is $\{2.87, 1.23, .39\}$mm. Field minimum at trap center is found out to be $4.67G$. The trap frequency along Z and theta direction are 166.13Hz and 767.99Hz, respectively. As number of planar wires are increased the trap center decreases and traps becomes shallower due to field cancellation from adjacent wires. To study tunneling we need the distance between the adjacent traps to be small which can only happen by increasing number of wires in this plane. In addition there is a 2d minimum between 3d traps as shown in fig.

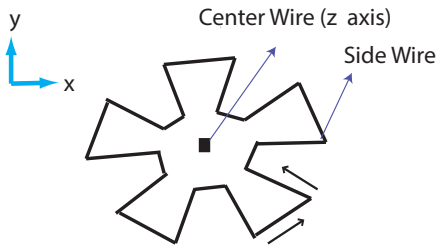

Figure 4.5: Design of magnetic trap I

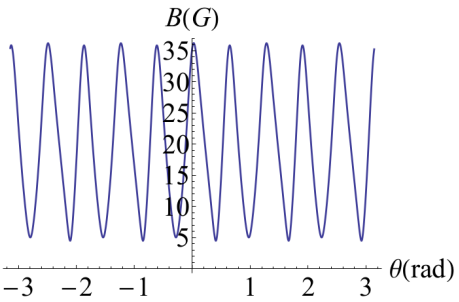

(a) Contour Plot for magnetic trap I

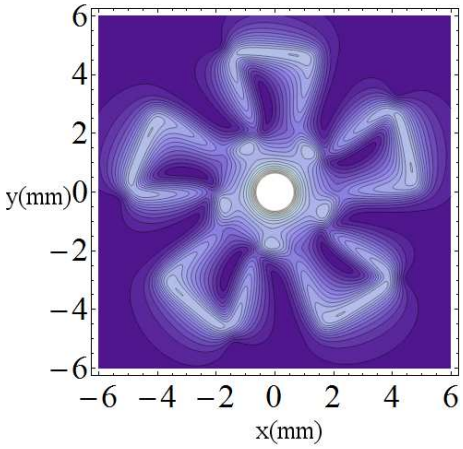

(b) Magnetic field along theta

Figure 4.6: Field Plot for magnetic trap I

4.6. So this type of design is not useful for our purpose.

4.2.2 Magnetic trap II

To avoid the problems mentioned in the previous trap, a new design is proposed. The above problem is avoided by adding circular wires to provide confinement in the x-direction rather than bending the side wires in the shape of z-wires. The design which creates circular array of magnetic field is shown in fig. 4.7. We consider the

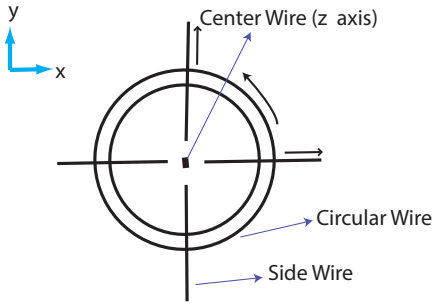

Figure 4.7: Design of magnetic trap II

length of side wires - 50mm, of center wire - 100mm. Radii of circular wire - 27mm and 34 mm, respectively. For the case if 4 side wire, the field plots along Z, θ and

radial direction is shown in fig. 4.8.

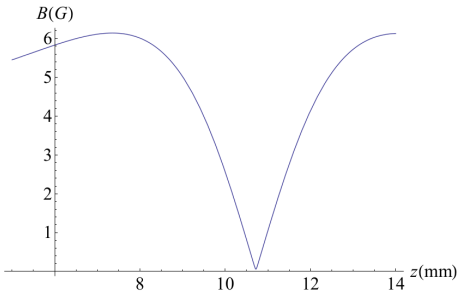

(a) Field variation in Z Axis

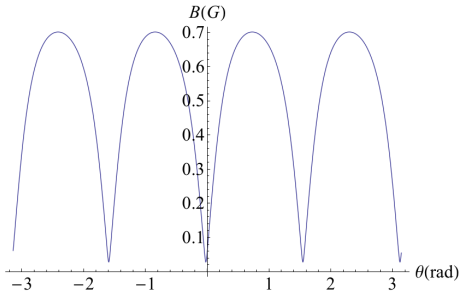

(b) Field variation in theta direction

Figure 4.8: Field variation along radial direction.

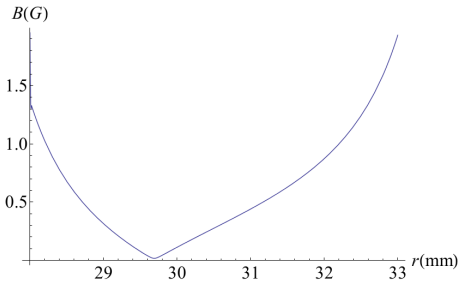

(a) Field Plot for magnetic trap II along different axes

4.3 Summary and Conclusion

Two and three dimensional micro traps are studied in detailed particularly U wire and Z wire. Field gradients and trap frequency variations are shown with the wire parameter. Later, rf dressed state theory is used to study adiabatic rf potentials. These rf-induced dressed state potentials are studied in detail for linear , circular and elliptic polarization. Later on we aimed to utilize this toolbox of rf dressed state to study circular array of magnetic trap. For this two different design are presented along with their drawbacks. Also physics of single particle are studied for periodic potential.

4.4 Future Direction

In the near future the aim is to study dynamics of atom in these new magnetic traps and variations of tunneling coefficients as a function of number of side wire in the traps. Study of RF dressed potential with such a circular lattice is one of the future research direction of this work.

Bibliography

[1] T. Schumm, S. Hofferberth, L. M. Andersson, S. Wildermuth, S. Groth, I. Bar-Joseph, J. Schmiedmayer, and P. Krüger, "Matter-wave interferometry in a double well on an atom chip," *Nature physics*, vol. 1, no. 1, pp. 57–62, 2005.

[2] W. Ketterle, D. Durfee, and D. Stamper-Kurn, "Making, probing and understanding bose-einstein condensates," *arXiv preprint cond-mat/9904034*, vol. 5, 1999.

[3] W. Ketterle, "Nobel lecture: When atoms behave as waves: Bose-einstein condensation and the atom laser," *Reviews of Modern Physics*, vol. 74, no. 4, pp. 1131–1151, 2002.

[4] F. Dalfovo, S. Giorgini, L. P. Pitaevskii, and S. Stringari, "Theory of bose-einstein condensation in trapped gases," *Reviews of Modern Physics*, vol. 71, no. 3, p. 463, 1999.

[5] E. A. Cornell and C. E. Wieman, "Nobel lecture: Bose-einstein condensation in a dilute gas, the first 70 years and some recent experiments," *Reviews of Modern Physics*, vol. 74, no. 3, p. 875, 2002.

[6] A. J. Leggett, "Bose-einstein condensation in the alkali gases: Some fundamental concepts," *Reviews of Modern Physics*, vol. 73, no. 2, p. 307, 2001.

[7] C. Pethick and H. Smith, *Bose-Einstein condensation in dilute gases*. Cambridge university press, 2002.

[8] T. W. Hänsch and A. L. Schawlow, "Cooling of gases by laser radiation," *Optics Communications*, vol. 13, no. 1, pp. 68–69, 1975.

[9] S. Chu, L. Hollberg, J. E. Bjorkholm, A. Cable, and A. Ashkin, "Three-dimensional viscous confinement and cooling of atoms by resonance radiation pressure," *Physical Review Letters*, vol. 55, no. 1, p. 48, 1985.

[10] E. Raab, M. Prentiss, A. Cable, S. Chu, and D. E. Pritchard, "Trapping of neutral sodium atoms with radiation pressure," *Physical Review Letters*, vol. 59, no. 23, p. 2631, 1987.

[11] W. Ketterle and N. Van Druten, "E vapora tive cooling of trapped atoms," *Advances in atomic, molecular, and optical physics*, vol. 37, p. 181, 1996.

[12] J. Reichel, "Microchip traps and bose–einstein condensation," *Applied Physics B*, vol. 74, no. 6, pp. 469–487, 2002.

[13] R. Folman, P. Krüger, J. Schmiedmayer, J. Denschlag, and C. Henkel, "Microscopic atom optics: from wires to an atom chip," *Advances in Atomic Molecular and Optical Physics*, vol. 48, pp. 263–356, 2002.

[14] J. Schmiedmayer, R. Folman, and T. Calarco, "Quantum information processing with neutral atoms on an atom chip," *Journal of Modern Optics*, vol. 49, no. 8, pp. 1375–1388, 2002.

[15] P. Treutlein, T. Steinmetz, Y. Colombe, B. Lev, P. Hommelhoff, J. Reichel, M. Greiner, O. Mandel, A. Widera, T. Rom, *et al.*, "Quantum information processing in optical lattices and magnetic microtraps," *Fortschritte der Physik*, vol. 54, no. 8-10, pp. 702–718, 2006.

[16] W. H. Wing, "On neutral particle trapping in quasistatic electromagnetic fields," *Progress in Quantum Electronics*, vol. 8, no. 3, pp. 181–199, 1984.

[17] W. Ketterle and D. Pritchard, "Trapping and focusing ground state atoms with static fields," *Applied Physics B*, vol. 54, no. 5, pp. 403–406, 1992.

[18] E. Majorana, "Atomi orientati in campo magnetico variabile," *Il Nuovo Cimento (1924-1942)*, vol. 9, no. 2, pp. 43–50, 1932.

[19] T. Bergeman, G. Erez, and H. J. Metcalf, "Magnetostatic trapping fields for neutral atoms," *Physical Review A*, vol. 35, no. 4, p. 1535, 1987.

[20] R. Frisch and E. Segre, "Über die einstellung der richtungsquantelung. ii," *Zeitschrift für Physik A Hadrons and Nuclei*, vol. 80, no. 9, pp. 610–616, 1933.

[21] D. E. Pritchard, "Cooling neutral atoms in a magnetic trap for precision spectroscopy," *Physical Review Letters*, vol. 51, no. 15, p. 1336, 1983.

[22] V. Bagnato, G. Lafyatis, A. G. Martin, E. Raab, and R. Ahmad-Bitar, "Continuous stopping and trapping of neutral atoms," *Physical review letters*, vol. 58, pp. 2194–2197, 1987.

[23] Y. Gott, M. Ioffe, and V. Tel'kovskii, "Nucl. fusion, suppi," *Pt*, vol. 3, p. 1045, 1962.

[24] J. Reichel, W. Hänsel, and T. Hänsch, "Atomic micromanipulation with magnetic surface traps," *Physical review letters*, vol. 83, no. 17, p. 3398, 1999.

[25] A. Haase, D. Cassettari, B. Hessmo, and J. Schmiedmayer, "Trapping neutral atoms with a wire," *PHYSICAL REVIEW-SERIES A-*, vol. 64, no. 4, pp. 043405–043405, 2001.

[26] C. C. Tannoudji, J. Dupont-Roc, and G. Grynberg, *Atom-Photon Interactions*. Wiley, 1992.

[27] E. Muskat, D. Dubbers, and O. Schärpf, "Dressed neutrons," *Physical review letters*, vol. 58, no. 20, p. 2047, 1987.

[28] C. C. Agosta, I. F. Silvera, H. T. C. Stoof, and B. Verhaar, "Trapping of neutral atoms with resonant microwave radiation," *Physical review letters*, vol. 62, no. 20, p. 2361, 1989.

[29] R. Spreeuw, C. Gerz, L. S. Goldner, W. Phillips, S. Rolston, C. Westbrook, M. Reynolds, and I. F. Silvera, "Demonstration of neutral atom trapping with microwaves," *Physical review letters*, vol. 72, no. 20, p. 3162, 1994.

[30] O. Zobay and B. Garraway, "Two-dimensional atom trapping in field-induced adiabatic potentials," *Physical review letters*, vol. 86, no. 7, p. 1195, 2001.

[31] Y. Colombe, E. Knyazchyan, O. Morizot, B. Mercier, V. Lorent, and H. Perrin, "Ultracold atoms confined in rf-induced two-dimensional trapping potentials," *EPL (Europhysics Letters)*, vol. 67, no. 4, p. 593, 2004.

[32] I. Lesanovsky, S. Hofferberth, J. Schmiedmayer, and P. Schmelcher, "Manipulation of ultracold atoms in dressed adiabatic radio-frequency potentials," *Physical Review A*, vol. 74, no. 3, p. 033619, 2006.

[33] I. Lesanovsky, T. Schumm, S. Hofferberth, L. M. Andersson, P. Krüger, and J. Schmiedmayer, "Adiabatic radio-frequency potentials for the coherent manipulation of matter waves," *Physical Review A*, vol. 73, no. 3, p. 033619, 2006.

[34] S. Hofferberth, I. Lesanovsky, B. Fischer, J. Verdu, and J. Schmiedmayer, "Radiofrequency-dressed-state potentials for neutral atoms," *Nature Physics*, vol. 2, no. 10, pp. 710–716, 2006.

[35] N. Ashcroft and N. Mermin, "Solid state physics wb saunders co," *Philadelphia, PA*, p. 701, 1976.

[36] D. Jaksch, C. Bruder, J. I. Cirac, C. W. Gardiner, and P. Zoller, "Cold bosonic atoms in optical lattices," *Physical Review Letters*, vol. 81, no. 15, p. 3108, 1998.